

## **Flatness-Based Decentralized Control of Bidirectional Interlink Power Converters in Grid-Connected Hybrid Microgrids Using Adaptive High-Gain PI-Observer**

Zolfaghari, Mahdi; Abedi, Mehrdad; Gharehpetian, Gevork B.; Guerrero, Josep M.

*Published in:*  
IEEE Systems Journal

*DOI (link to publication from Publisher):*  
[10.1109/JSYST.2020.2977660](https://doi.org/10.1109/JSYST.2020.2977660)

*Publication date:*  
2021

*Document Version*  
Accepted author manuscript, peer reviewed version

[Link to publication from Aalborg University](#)

*Citation for published version (APA):*  
Zolfaghari, M., Abedi, M., Gharehpetian, G. B., & Guerrero, J. M. (2021). Flatness-Based Decentralized Control of Bidirectional Interlink Power Converters in Grid-Connected Hybrid Microgrids Using Adaptive High-Gain PI-Observer. *IEEE Systems Journal*, 15(1), 478-486. Article 9052664.  
<https://doi.org/10.1109/JSYST.2020.2977660>

### **General rights**

Copyright and moral rights for the publications made accessible in the public portal are retained by the authors and/or other copyright owners and it is a condition of accessing publications that users recognise and abide by the legal requirements associated with these rights.





- Users may download and print one copy of any publication from the public portal for the purpose of private study or research.
- You may not further distribute the material or use it for any profit-making activity or commercial gain
- You may freely distribute the URL identifying the publication in the public portal -

### **Take down policy**

If you believe that this document breaches copyright please contact us at [vbn@aub.aau.dk](mailto:vbn@aub.aau.dk) providing details, and we will remove access to the work immediately and investigate your claim.



# Flatness-Based Decentralized Control of Bidirectional Interlink Power Converters in Grid-Connected Hybrid Microgrids Using Adaptive High-Gain PI-Observer

Mahdi Zolfaghari , *Member, IEEE*, Mehrdad Abedi , *Member, IEEE*,  
Gevork B. Gharehpetian , *Senior Member, IEEE*, and Josep M. Guerrero , *Fellow, IEEE*

**Abstract**—This article studies the control of bidirectional interlink power converters (BILPCs) in hybrid microgrids (HMGs). Here, the BILPCs interconnect a dc microgrid to an ac microgrid in a grid-connected HMG. Thanks to the flatness property of differential equations of BILPCs, the control method is able to provide desirable output characteristics and robustness against unmodeled dynamics and unknown inputs. First, the flat models of single BILPC and parallel-connected BILPCs are determined. Second, to approximate the unknown inputs and disturbances such as changes in the controlled output voltages of BILPCs, an adaptive high-gain proportional-integral observer is designed for BILPCs. Based on a linear quadratic regulation approach, the high gains of this observer change dynamically during the approximation process, to achieve the best result. Third, the approximated parameters are implemented in the design process of sliding mode control-based decentralized controllers for BILPCs. The simulations confirm the capability of the new method considering the dynamic response and power transferring control capability among the ac and dc microgrids.

**Index Terms**—Adaptive proportional-integral (PI) disturbance observer, flatness, hybrid microgrid (HMG), interlink power converter.

## I. INTRODUCTION

OWING to having many technical benefits and being environment-friendly, renewable energy sources (RESs) have obtained much research attention in the last decade [1]. As it is well-confirmed, the best way to imbed low-scale RESs into current power systems is integrating them in microgrids [2]. The microgrids facilitate the management and operation of RESs, energy storage systems (ESSs), and regional loads. The ac and dc microgrids have been investigated in the literature well [3]. The

Manuscript received September 22, 2019; revised February 7, 2020; accepted February 25, 2020. The work of Josep M. Guerrero was funded by The Villum Fonden under Villum Investigator Grant 25920. The work of M. Zolfaghari and G. B. Gharehpetian was supported by the Elite National Foundation of Iran. (Corresponding author: Mehrdad Abedi.)

Mahdi Zolfaghari, Mehrdad Abedi, and Gevork B. Gharehpetian are with the Department of Electrical Engineering, Amirkabir University of Technology, Tehran, Iran (e-mail: mahdizolfaghari@aut.ac.ir; abedi@aut.ac.ir; grptian@aut.ac.ir).

Josep M. Guerrero is with the Center of Research on Microgrids, Department of Energy Technology, Aalborg University, 9220 Aalborg East, Denmark (e-mail: joz@et.aau.dk).

Digital Object Identifier 10.1109/JSYST.2020.2977660

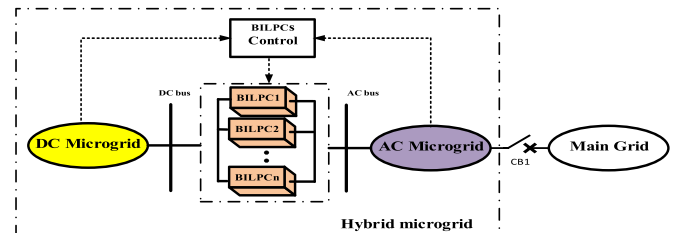


Fig. 1. Typical grid-connected HMG, interconnected by BILPCS.

hybrid microgrids (HMGs), which is a combination of both ac and dc microgrids, is getting more interest in current research because they have the advantages of both ac and dc microgrids simultaneously. As declared, the HMGs are the main structure for interconnecting ac and dc loads/sources in future smart grids [4], [5]. An exemplary grid-tied HMG is indicated in Fig. 1. It includes at least two microgrids; one ac microgrid and one dc microgrid which are interconnected through bidirectional interlink power converters (BILPCs) with a control strategy. The dc microgrid can include different dc sources such as photovoltaic (PV) equipped with battery storage to grant regional loads. Similarly, the ac microgrid can include wind turbine and regional loads. In this study, the HMG is tied to a sturdy upstream ac bus, i.e., the main grid. Therefore, the voltage and frequency of the HMG is regulated by the main grid and thus, the HMG works in power control mode to transfer power with the power system [6], [7].

Through the BILPCs, the ac and dc microgrids can transfer power when needed. To enhance the reliability and also the amount of transferred power, the BILPCs are connected in parallel [8], [9]. However, after interconnecting the ac and dc microgrids using BILPCs, some problems arise as follows: 1) The dc bus of a BILPC is tied to a fluctuating dc link, i.e., the dc subgrid. This makes the exchanged power oscillatory since the transferred power among microgrids closely relies on the dc-link voltage amplitude [5], [10]. 2) The HMG includes different components with various dynamics. In this surrounding, setting of the same value for the output voltages and frequencies of BILPCs is a great problem to remove diffusive current and losses [11]. 3) Variation in the model specifications, for example, transmission line resistance, etc., influence the power sharing

performance among BILPCs and exchanged power [12]. 4) It is forecasted to have balanced power distribution between BILPCs when the BILPCs have equal power ratings [13]. 5) If a fault appears in the dc or ac subsystem, the current is unequally divided between the BILPCs. Therefore, the current passing through a BILPC can break the constraints, resulting in brownout of the BILPC. Thus, the volume of the transferred power is diminished which increases unsupplied energy in a microgrid [14]. 6) The exchanged power between microgrids may oscillate due to the variable output power of some RESs, which are located in ac or dc microgrids [15]. 7) The harmonic distortions cause phase differences among parallel-connected BILPCs, which in turn result in power losses and voltage drop [16]. 8) The BILPCs can work with various power factors, which causes fluctuations in transferring power [17].

To resolve the above-mentioned problems, many efforts have been reported in the literature. The researchers in [18] have presented a hierarchical control strategy for BILPCs. The first control stage has used a droop scheme, while the secondary stage has tried to delete the errors created by the first stage controllers. The third control stage is dedicated to control the power transferring among the HMG and the power system. The main problem of this strategy is that a tradeoff among the dc voltage fluctuations and the power distribution capability should be held. In [19], based on the stationary reference frame, a control scheme has been described for ILCs. The method facilitates the application of harmonic compensators and avoids cross-coupling among axes. Fliess *et al.* in [20] have presented a correlative control strategy for an HMG. The stochastic output of renewable resources was studied and the control strategy tried to arrange a swift power transferring among microgrids while keeping stability criterion. The studied HMG model was a simplified one and the proportional-integral (PI) controllers have not been tuned optimally. The effects of extraneous distortions, for example, voltage distortion on operation of BILPCs were investigated in [21]. The voltage fluctuations cause power transfer oscillations and as a result, the current passing through the BILPCs can break the constraints and cause BILPC outage. Therefore, the researchers assigned one BILPC as superfluous converter with higher nominal parameters and using the positive, negative, and zero sequences concepts, described an additive unbalance part cancellation scheme to control the BILPCs. The strategy, however, is not capable of diminishing the reactive power fluctuations. A control scheme according to droop control concept was described in [22]. It has been indicated that an unreal impedance has been able to modify the small-signal properties of HMGs. By implementation of ESSs, a self-governing control strategy was presented in [23] to control the BILPCs, keeping the HMG stable in grid-forming operation. In [24], a sturdy  $H_\infty$ -based controller was described for parallel distributed generations, which represented logical power distribution.

The purpose of this article is to present a novel control strategy for BILPCs based on flatness concept and observer-based control theory. The major merit of flatness-based control strategies is that dynamic response of state variables in steady state as well as transient state is known. This property makes design process straightforward and easy to follow since system trajectories are predefined [25]. To implement the flatness-based controllers, an approximation of unknown inputs, disturbances, and unmeasured

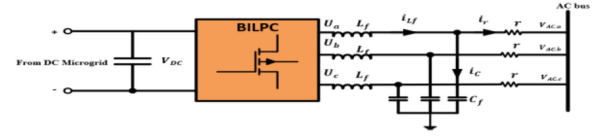


Fig. 2. Electric circuit model of BILPC.

states is necessary. To this end, an adaptive high-gain PI-observer is designed in this article. The high gains of this observer vary dynamically during the estimation process to have the best approximation results. Therefore, having the flat model of the BILPCs and the approximation of essential parameters, the system model is input–output (I/O) linearized and the sliding mode control (SMC)-based feedback controllers are designed based on the desired trajectories. A typical HMG is taken as an example to show the effectiveness of the proposed approach.

The reminder parts of this article are arranged as follows: the flat model of a single BILPC as well as parallel-connected BILPCs are obtained in Section II. The overall description of the proposed control strategy is also given in this section. After that, the design process of the adaptive high-gain PI-disturbance observer is detailed in Section III. Then, I/O linearization of model of BILPCs and the SMC-based controllers design process are discussed in Section IV. Later on, the simulation results and case studies are presented in Section V, where an exemplary HMG is considered as system under study. At last, conclusion remarks are introduced in Section VI.

## II. FLAT MODEL OF BILPCs AND GENERAL STRUCTURE OF PROPOSED CONTROL STRATEGY

The flatness concept was derived from differential algebra and first introduced in [26]. In differential algebra terminology, a dynamic system is flat if one can find a collection of variables, namely flat output elements, so that without needing integration, all state variables and inputs elements can be extracted from the flat output elements. Mathematically, if  $x \in \mathbb{R}^n$  is the vector of state variables,  $u \in \mathbb{R}^m$  the input vector, and  $y \in \mathbb{R}^m$  the output vector, then the system is flat if we can write [26]

$$x = \phi(y, \dot{y}, \dots, y^{(r)}) \quad (1)$$

$$u = \varphi(y, \dot{y}, \dots, y^{(r+1)}) \quad (2)$$

$$y = \psi(x, u, \dot{u}, \dots, u^{(l)}) \quad (3)$$

where  $\text{rank}(\psi) = n$ ,  $\text{rank}(\varphi) = m$ , and  $\text{rank}(\phi) = m$ . In the following two sections, we demonstrate that (1)–(3) hold for a single BILPC and parallel-connected BILPCs. Then, general structure of the proposed strategy will be described.

### A. Flat Model of a Single BILPC With Uncertainties

Fig. 2 illustrates the circuit representation of a BILPC which is located between a dc bus and an ac bus. In inverter mode, the BILPC alters the dc voltage of dc subgrid,  $V_{DC}$ , to a three-phase ac voltage,  $U_{abc}$ , according to SPWM strategy. Also, when working as a rectifier, the BILPC alters the ac voltage of the subgrid to a dc voltage. This property allows a bidirectional power transferring

among the subgrids.  $U_{abc}$  is the controlled output voltage of the BILPC. The letter “ $U$ ” is used to distinguish the controlled voltage when designing the observer and SMC-based controllers in the next sections. The BILPC is tied to ac microgrid, with voltage of  $V_{AC,abc}$ , through an  $LC$  filter ( $L_f$ , and  $C_f$ ), and a nearly resistive line impedance,  $r$ . Note that in a real microgrid, the line impedance is dominantly resistive. Using KVL and KCL circuit laws, we have

$$V_{L_f,abc} = U_{abc} - V_{C,abc} \quad (4)$$

$$V_{r,abc} = V_{C,abc} - V_{AC,abc} \quad (5)$$

$$i_{C,abc} = i_{L_f,abc} - i_{r,abc}. \quad (6)$$

Here, the voltages and currents are denoted in Fig. 2. Implementing Clarke transformation, (4) and (6) can be transformed into the  $\alpha\beta$  coordination

$$\frac{di_{L_f,\alpha}}{dt} = \frac{1}{L_f} (U_\alpha - V_{C,\alpha}) \quad (7)$$

$$\frac{di_{L_f,\beta}}{dt} = \frac{1}{L_f} (U_\beta - V_{C,\beta}) \quad (8)$$

$$\frac{dV_{C,\alpha}}{dt} = \frac{1}{C_f} (i_{L_f,\alpha} - i_{r,\alpha}) \quad (9)$$

$$\frac{dV_{C,\beta}}{dt} = \frac{1}{C_f} (i_{L_f,\beta} - i_{r,\beta}). \quad (10)$$

Defining the parametric uncertainties, as follows, and using linear fractional transformation, we obtain the following:

$$\frac{1}{L_f} = \frac{1}{\bar{L}_f (1 + \rho_{L_f} \delta_{L_f})} = \frac{1}{\bar{L}_f} - \frac{\rho_{L_f}}{\bar{L}_f} (1 + \rho_{L_f} \delta_{L_f})^{-1} \quad (11)$$

$$\frac{1}{C_f} = \frac{1}{\bar{C}_f (1 + \rho_{C_f} \delta_{C_f})} = \frac{1}{\bar{C}_f} - \frac{\rho_{C_f}}{\bar{C}_f} (1 + \rho_{C_f} \delta_{C_f})^{-1} \quad (12)$$

where  $\bar{L}_f$  and  $\bar{C}_f$  are the rated values of the output  $LC$  filter inductor and capacitor,  $\rho_{L_f}$ ,  $\delta_{L_f}$ ,  $\rho_{C_f}$ ,  $\delta_{C_f}$  represent the probable relative disturbances on  $L_f$  and  $C_f$ , respectively, and can be obtained using worst-case analysis. Also, the uncertainty on the controlled output voltage is considered as

$$U_{abc} = \bar{U}_{abc} + \rho_{U_{abc}} \Delta U_{abc} \quad (13)$$

where  $\rho_{U_{abc}} \Delta U_{abc}$  indicates the deviated additive term consisted in the output voltage and  $\bar{U}_{abc}$  represents the rated parameter. Notice that the controlled parameter includes distorted terms because the dc bus is tied to a fluctuating dc voltage, i.e., the dc subgrid. Note that (13) in the  $\alpha\beta$  coordination is as follows:

$$U_\alpha = \bar{U}_\alpha + \rho_{U_\alpha} \Delta U_\alpha \quad (14)$$

$$U_\beta = \bar{U}_\beta + \rho_{U_\beta} \Delta U_\beta. \quad (15)$$

Substituting (11)–(15) into (7)–(10) gives the perturbed model of the BILPC

$$\begin{aligned} \frac{di_{L_f,\alpha}}{dt} = & \frac{1}{\bar{L}_f} U_\alpha - \frac{1}{\bar{L}_f} V_{C,\alpha} \\ & + \underbrace{\left[ \frac{1}{\bar{L}_f} \rho_{U_\alpha} - \frac{\rho_{L_f} \rho_{U_\alpha}}{\bar{L}_f} (1 + \rho_{L_f} \delta_{L_f})^{-1} \right]}_{a_1} \Delta U_\alpha \\ & + \underbrace{\left[ \frac{\rho_{L_f}}{\bar{L}_f} (1 + \rho_{L_f} \delta_{L_f})^{-1} (V_{C,\alpha} - U_\alpha) \right]}_{d_1} \end{aligned} \quad (16)$$

$$\begin{aligned} \frac{di_{L_f,\beta}}{dt} = & \frac{1}{\bar{L}_f} U_\beta - \frac{1}{\bar{L}_f} V_{C,\beta} \\ & + \underbrace{\left[ \frac{1}{\bar{L}_f} \rho_{U_\beta} - \frac{\rho_{L_f} \rho_{U_\beta}}{\bar{L}_f} (1 + \rho_{L_f} \delta_{L_f})^{-1} \right]}_{a_2} \Delta U_\beta \\ & + \underbrace{\left[ \frac{\rho_{L_f}}{\bar{L}_f} (1 + \rho_{L_f} \delta_{L_f})^{-1} (V_{C,\beta} - U_\beta) \right]}_{d_2} \end{aligned} \quad (17)$$

$$\begin{aligned} \frac{dV_{C,\alpha}}{dt} = & \frac{1}{\bar{C}_f} i_{L_f,\alpha} \\ & \times \underbrace{- \frac{\rho_{C_f}}{\bar{C}_f} (1 + \rho_{C_f} \delta_{C_f})^{-1} (i_{L_f,\alpha} - i_{r,\alpha}) - \frac{1}{\bar{C}_f} i_{r,\alpha}}_{d_3} \end{aligned} \quad (18)$$

$$\begin{aligned} \frac{dV_{C,\beta}}{dt} = & \frac{1}{\bar{C}_f} i_{L_f,\beta} \\ & \times \underbrace{- \frac{\rho_{C_f}}{\bar{C}_f} (1 + \rho_{C_f} \delta_{C_f})^{-1} (i_{L_f,\beta} - i_{r,\beta}) - \frac{1}{\bar{C}_f} i_{r,\beta}}_{d_4}. \end{aligned} \quad (19)$$

We define the state variables as  $\mathbf{x} = [x_1 \ x_2 \ x_3 \ x_4]^T = [i_{L_f,\alpha} \ i_{L_f,\beta} \ V_{C,\alpha} \ V_{C,\beta}]^T$ , input vector  $\mathbf{u} = [u_1 \ u_2]^T = [U_\alpha \ U_\beta]^T$  and the vector of the flat output  $\mathbf{y} = [y_1 \ y_2]^T = [0 \ 0 \ 1 \ 1][x_1 \ x_2 \ x_3 \ x_4]^T$ . Also, because the flat outputs of a flat system are not unique, to minimize the energy saved in the  $LC$  filter and therefore to reduces the filter size, the following auxiliary flat output is defined:

$$\begin{aligned} z_1 = & \omega \bar{L}_f (1 + \rho_{L_f} \delta_{L_f}) (i_{L_f,\alpha}^2 + i_{L_f,\beta}^2) \\ & - \omega \bar{C}_f (1 + \rho_{C_f} \delta_{C_f}) (V_{C,\alpha}^2 + V_{C,\beta}^2) \end{aligned} \quad (20)$$

which shows the subtraction of the energy saved in inductance and capacitor of the filter.  $\omega$  is the angular frequency in rad/s.

Now, the flatness of the BILPC model will be discussed. Since we have

$$y_1 = V_{C,\alpha} = x_3 \quad (21)$$

$$y_2 = V_{C,\beta} = x_4 \quad (22)$$

therefore

$$x_3 = \phi_1(y_1) \quad (23)$$

$$x_4 = \phi_2(y_2). \quad (24)$$

Also, using (18)

$$x_1 = \dot{y}_1 + i_{r,\alpha} - \bar{C}_f d_3. \quad (25)$$

Thus

$$x_1 = \phi_3(\dot{y}_1) \quad (26)$$

$$\dot{x}_1 = \phi_4(\dot{y}_1, \ddot{y}_1). \quad (27)$$

In a similar way, using (19) we obtain the following:

$$x_2 = \dot{y}_2 + i_{r,\beta} - \bar{C}_f d_4. \quad (28)$$

And we can write

$$x_2 = \phi_5(\dot{y}_2) \quad (29)$$

$$\dot{x}_2 = \phi_6(\dot{y}_2, \ddot{y}_2). \quad (30)$$



Therefore, (1) holds. From (16), we have the following:

$$U_\alpha = \bar{L}_f \dot{x}_1 + y_1 - a_1 \bar{L}_f \Delta U_\alpha - \bar{L}_f d_1. \quad (31)$$

Thus

$$U_\alpha = \varphi_1(y_1, \dot{y}_1, \ddot{y}_1). \quad (32)$$

Similarly, from (17) we obtain the following:

$$U_\beta = \bar{L}_f \dot{x}_2 + y_2 - a_2 \bar{L}_f \Delta U_\beta - \bar{L}_f d_2 \quad (33)$$

$$U_\beta = \varphi_1(y_2, \dot{y}_2, \ddot{y}_2). \quad (34)$$

Therefore, (2) holds. Furthermore, from (16) we can see that

$$y_1 = -\bar{L}_f \dot{x}_1 + U_\alpha + \bar{L}_f a_1 \Delta U_\alpha + \bar{L}_f d_1. \quad (35)$$

Thus

$$y_1 = \psi_1(x, u). \quad (36)$$

From (17) we also have

$$y_2 = -\bar{L}_f \dot{x}_2 + U_\beta + \bar{L}_f a_2 \Delta U_\beta + \bar{L}_f d_2. \quad (37)$$

Thus

$$y_2 = \psi_2(x, u). \quad (38)$$

Therefore, (3) holds.

For the auxiliary output, based on (20)–(22), (26), and (29), we also have

$$\begin{aligned} z_1 = & \omega \bar{L}_f (1 + \rho_{Lf} \delta_{Lf}) (\phi_3^2(\dot{y}_1) + \phi_5^2(\dot{y}_2)) \\ & - \omega \bar{C}_f (1 + \rho_{Cf} \delta_{Cf}) (y_1^2 + y_2^2). \end{aligned} \quad (39)$$

And we can write

$$z_1 = Z(y_1, y_2, \dot{y}_1, \dot{y}_2). \quad (40)$$

According to the analysis above, one can infer that the BILPC model is flat. Therefore, it can enjoy the flatness properties to design simple feedback controllers by applying I/O linearization. Thus, the BILPC can be represented as a flat MIMO system.

### B. Flat Model of Parallel-Connected BILPCs

Considering a system of  $n$  BILPCs, connected in parallel, it can be easily shown that the system is flat, following the similar concept described in the previous section. Note that each BILPC model is the same as one illustrated in Fig. 2. Defining the control vector, flat outputs, and auxiliary outputs as follows:

$$U = [U_\alpha^1 \ U_\alpha^2 \ \dots \ U_\alpha^n \ U_\beta^1 \ U_\beta^2 \ \dots \ U_\beta^n]^T_{(2n \times 1)} \quad (41)$$

$$Y = [y_1^1 \ y_1^2 \ \dots \ y_1^n \ y_2^1 \ y_2^2 \ \dots \ y_2^n]^T_{(2n \times 1)} \quad (42)$$

$$Z = [z_1^1 \ z_1^2 \ \dots \ z_1^n]^T_{(n \times 1)}. \quad (43)$$

Therefore, it can be demonstrated that all state variables and control inputs can be expressed as a function of flat output  $Y$  (its components) and its derivatives; thus, the system is flat.

### C. Proposed Control Strategy

To control parallel-connected BILPCs, we present a decentralized SMC scheme according to the implementation of an adaptive high-gain proportional-integral observer (AHGPIO). The overall block diagram of the novel scheme for each BILPC is illustrated in Fig. 3. As shown, first the disturbance/unknown inputs and unmeasured states,  $\Delta u$  and  $\hat{x}$ , are approximated using the AHGPIO. The I/O linearization are applied and virtual control signal vector  $V$ , based on the desired trajectories  $y_{\text{planned}}$ , is generated

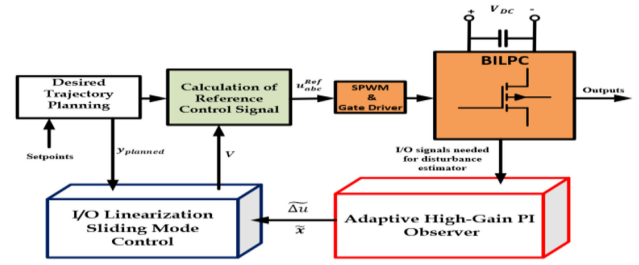


Fig. 3. General schematic representation of the novel control method for each BILPC.

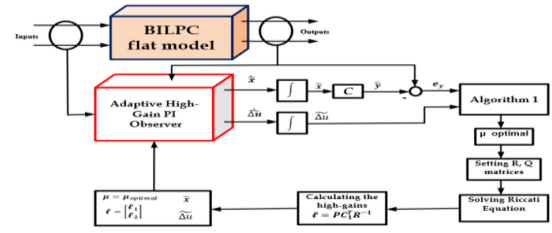


Fig. 4. Representation of designing process of proposed AGHPIO for BILPC.

using SMC. The desired trajectories can be predefined, thanks to the flatness of the system model. It should be noted that through defining the desired trajectories, all parallel-connected BILPCs can be coordinated. This is due to the fact that the same set-points and output voltages can be planned for each BILPC. Finally, the reference signals  $u_{abc}^{\text{Ref}}$  are generated and applied to the SPWM block of BILPC.

### III. DESIGNING OF ADAPTIVE HIGH-GAIN PI-OBSERVER

In order to apply I/O linearization and design the decentralized controllers, the unknown inputs and unmeasurable states need to be approximated first. To do this, an AHGPIO is implemented. As reported, the unknown inputs of an uncertain system can successfully be approximated by using high gains of PI observers [27]. However, choosing very large gains may result in fatal problems with respect to unmodeled dynamics and measurement disturbances and ruins the approximation result. Thus, to obtain the best result, the gains of the PI-observer vary during the approximation process, keeping the optimal values for the high-gains of the PI-observer. The topology of the novel AHGPIO is indicated in Fig. 4. As shown, based on an optimal procedure, the weighting matrices and high gains of the PI-observer are determined. The designing steps are as follows.

*Step 1:* The uncertain model of the BILPC, (16)–(19), is arranged as the standard form as follows:

$$\dot{x} = Ax + Bu + N\Delta u + Ed \quad (44)$$

$$y = Cx + h \quad (45)$$

where  $A_{n \times n}$ ,  $B_{n \times l}$ , and  $C_{m \times n}$  are the system matrices,  $\Delta u$  is the unknown inputs,  $d$  is the unmodeled dynamics,  $h$  the measurement noise,  $E_{r \times p}$  and  $N_{n \times r}$  are coefficient matrices. Accordingly, for

the uncertain model of the BILPC, we have

$$A = \begin{bmatrix} 0 & 0 & -\frac{1}{L_f} & 0 \\ 0 & 0 & 0 & -\frac{1}{L_f} \\ \frac{1}{C_f} & 0 & 0 & 0 \\ 0 & \frac{1}{C_f} & 0 & 0 \end{bmatrix}, B = \begin{bmatrix} \frac{1}{L_f} & 0 \\ 0 & \frac{1}{L_f} \\ 0 & 0 \\ 0 & 0 \end{bmatrix}$$

$$C = [0 \ 0 \ 1 \ 1], N = \begin{bmatrix} a_1 & 0 \\ 0 & a_2 \\ 0 & 0 \\ 0 & 0 \end{bmatrix}, E = \begin{bmatrix} 1 & 0 & 0 & 0 \\ 0 & 1 & 0 & 0 \\ 0 & 0 & 1 & 0 \\ 0 & 0 & 0 & 1 \end{bmatrix}$$

$$\Delta u = [\Delta U_\alpha \Delta U_\beta]^T, d = [d_1 \ d_2 \ d_3 \ d_4]^T. \quad (46)$$

*Step 2:* The observer dynamics are defined as follows:

$$\begin{bmatrix} \dot{\tilde{x}} \\ \dot{\tilde{\Delta}u} \end{bmatrix} = \underbrace{\begin{bmatrix} A & N \\ 0 & 0 \end{bmatrix}}_{A_1} \begin{bmatrix} \tilde{x} \\ \tilde{\Delta}u \end{bmatrix} + \underbrace{\begin{bmatrix} B \\ 0 \end{bmatrix}}_{B_1} u + \underbrace{\begin{bmatrix} \ell_1 \\ \ell_2 \end{bmatrix}}_{\ell} (y - \tilde{y}) \quad (47)$$

$$\tilde{y} = \underbrace{\begin{bmatrix} C & 0 \end{bmatrix}}_{C_1} \begin{bmatrix} \tilde{x} \\ \tilde{\Delta}u \end{bmatrix}. \quad (48)$$

From (47) and (48), one should note that the observer is defined as an extended system, i.e., the unknown inputs  $\Delta u$  is considered as an additional state. Thus, to design the observer, the extended dynamic model  $(A_1, C_1)$  must be observable so that the following condition for all eigenvalues  $\lambda$  is satisfied:

$$\text{rank} \begin{bmatrix} \lambda I_n & -N \\ 0 & \lambda I_r \\ C & 0 \end{bmatrix} = n + r. \quad (49)$$

*Step 3:* The errors are defined as follows:

$$e_x = \tilde{x} - x \quad (50)$$

$$e_{\Delta u} = \tilde{\Delta}u - \Delta u. \quad (51)$$

Thus, based on (47) and (48), the errors dynamics become

$$\begin{bmatrix} \dot{e}_x \\ \dot{e}_{\Delta u} \end{bmatrix} = \underbrace{\begin{bmatrix} A - \ell_1 C & N \\ -\ell_2 C & 0 \end{bmatrix}}_{A_{1e}} \begin{bmatrix} e_x \\ e_{\Delta u} \end{bmatrix} - \underbrace{\begin{bmatrix} E d \\ \Delta u \end{bmatrix}}_{\ell} + \underbrace{\begin{bmatrix} \ell_1 \\ \ell_2 \end{bmatrix}}_{\ell} h. \quad (52)$$

Therefore, to have a reasonable observer design, the errors have to be zero (i.e.,  $e_x, e_{\Delta u} \rightarrow 0$ ). This is possible by choosing appropriate feedback matrix  $\ell$ , i.e., the high gains of the PI-observer. Decoupling the error dynamics, by using Laplace Transform, we obtain the following:

$$E_x(s) = [sI - (A - \ell_1 C)]^{-1} N E_{\Delta u}(s) - [sI - (A - \ell_1 C)]^{-1} E D(s) + [sI - (A - \ell_1 C)]^{-1} \ell_1 H(s) \quad (53)$$

$$E_{\Delta u}(s) = -[sI + \ell_2 C[sI - (A - \ell_1 C)]^{-1} N]^{-1} s \Delta U(s) + [sI + \ell_2 C[sI - (A - \ell_1 C)]^{-1} N]^{-1} \ell_2 C \times [sI - (A - \ell_1 C)]^{-1} E D(s) + [sI + \ell_2 C[sI - (A - \ell_1 C)]^{-1} N]^{-1} \times \ell_2 [I - C[sI - (A - \ell_1 C)]^{-1} \ell_1] H(s). \quad (54)$$

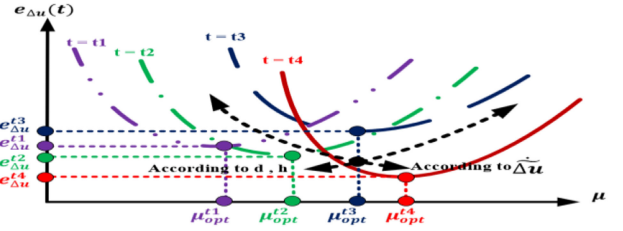


Fig. 5. Relationship between design parameter  $\mu$  and unknown input error  $e_{\Delta u}$ .

Therefore, based on (54), to minimize the effects of unknown inputs on the approximation results, the following condition must be satisfied:

$$\left\| [sI + \ell_2 C[sI - (A - \ell_1 C)]^{-1} N]^{-1} \right\|_{\infty} \leq \varepsilon \quad (55)$$

where  $\varepsilon$  is a sufficiently small value.

*Step 4:* Based on the LQR method, the high-gains of the AHGPIO are obtained by solving the following equation:

$$\ell = P C_1^T R^{-1} \quad (56)$$

in (56),  $P$  is determined by solving the Riccati equation

$$A_1 P + P A_1^T + Q - P C_1^T R^{-1} C_1 P = 0. \quad (57)$$

Before solving the above equation, the weighting matrices  $R$  and  $Q$  must appropriately be selected.

*Step 5:* For the purpose of making the high-gains adaptive, it is assumed that the weighting matrices have the following forms:

$$R = \partial I_m \quad (58)$$

$$Q = \mu \begin{bmatrix} \mu^{-1} I_n & 0 \\ 0 & I_r \end{bmatrix} \quad (59)$$

where  $\partial, \mu > 0$ . As described in [27], the main characteristics of choosing the weighting functions are reflected in positive parameter  $\mu$ . Here, we let  $\mu$  is chosen based on Algorithm 1 (which is described in the next step). In this algorithm,  $\tau$  is the integration time step, and  $\gamma$  is a positive constant. First, a random initial value is chosen for  $\mu$ . Then, the objective function value for  $\mu = \mu_{\text{main}} = \mu_{\text{initial}}$ , and its lower and upper bounds are evaluated. We let  $\theta_l = 0.1\mu_{\text{main}}$  and  $\theta_u = 10\mu_{\text{main}}$ . If the objective function is minimum for chosen  $\mu$ , then this current value and approximation are accepted and integration goes on. Otherwise, a new value for  $\mu$  is set up and the integration is repeated. This process proceeds until an optimal value is obtained for  $\mu$ . Fig. 5 illustrates the relationship between the design parameter  $\mu$  and the unknown input error. As demonstrated, according to the unknown inputs and unmodeled dynamics and measurement disturbances, the absolute value of  $e_{\Delta u}$  varies with time and  $\mu$ . However, at each instant  $t$ , there is a point at which the error is minimum for a specific value of  $\mu = \mu_{\text{optimal}}$ , which is a point that gives the minimum cost function.

*Step 6:* When  $\mu_{\text{optimal}}$  is determined from the previous step, then the weighting matrices (58) and (59) are available and therefore, Riccati equation (57) can be solved for  $P$ . In order to find the response of (57) numerically, we can use Schur method or Newtonian methods. However, here we assume that the solution

**Algorithm 1:**


---

```

a) Set  $\mu = \mu_{main}$  % random initial value for  $\mu$ ,
    $\mu_{main} = \mu_{initial}$ .
b) Set  $\begin{cases} \mu_{lower} = \theta_l \mu_{main} \% \text{Lower band} \\ \mu_{upper} = \theta_u \mu_{main} \% \text{Upper band} \end{cases}$ 
c) Evaluate the quadratic objective function:
    $f_{min} = \min_{\mu_{lower} \cdot \mu_{main} \cdot \mu_{upper}} f = \gamma \tau e_y^2(t) + \|\ell_2\|_{Frobenius}^2$ 
if  $f_{min} = f_{main}$ 
    $\mu_{optimal} = \mu_{main}$ 
    $t = t + \tau$ ;
    $i = i + 1$ ;
else
   set a new value for  $\mu_{main}$ 
    $t = t$ ;
    $i = i$ ;
d) go to (b)
end
 $\mu = \mu_{optimal}$ 

```

---

is analytically determined as follows:

$$P = \begin{bmatrix} P_{11} & P_{12} \\ P_{12}^T & P_{22} \end{bmatrix}. \quad (60)$$

Therefore, substituting (58)–(60) into (57) we obtain

$$AP_{11} + NP_{12}^T + P_{11}A^T + P_{12}N^T + I_n = P_{11}C^T C \partial^{-1} P_{11} \quad (61)$$

$$AP_{12} + NP_{12} = P_{11}C^T C \partial^{-1} P_{12} \quad (62)$$

$$P_{12}^T A^T + P_{12}N^T = P_{12}^T C^T C \partial^{-1} P_{11} \quad (63)$$

$$\mu I_r = P_{12}^T C^T C \partial^{-1} P_{12} \quad (64)$$

and the response of (56), i.e., the high-gains, is as follows:

$$\ell = \begin{bmatrix} \ell_1 \\ \ell_2 \end{bmatrix} = \begin{bmatrix} P_{11} & P_{12} \\ P_{12}^T & P_{22} \end{bmatrix} \begin{bmatrix} C^T \\ 0 \end{bmatrix} \partial^{-1} = \begin{bmatrix} P_{11}C^T \partial^{-1} \\ P_{12}^T C^T \partial^{-1} \end{bmatrix}. \quad (65)$$

Therefore, these feedback high-gain matrices drift the errors to zero.

#### IV. DECENTRALIZED SMC-BASED CONTROL DESIGN

After approximating the unmeasured states and unknown inputs, these estimated parameters are used for I/O model linearization and designing the SMC-based decentralized controllers. Therefore, in the following two sections, first the linearized model of the BILPC is determined and then the controllers are designed. At the last section, the process of obtaining the proposed desired trajectories is discussed.

##### A. I/O linearization of BILPC Model

For the first flat output,  $y_1$ , since its relative degree is 2, we have

$$\dot{y}_1 = \dot{x}_3 \Rightarrow \ddot{y}_1 = \ddot{x}_3 = \frac{1}{C_f} \dot{x}_3 + \dot{d}_3. \quad (66)$$

Using (16) and the approximated parameters

$$\ddot{y}_1 = -\frac{1}{C_f \bar{L}_f} \tilde{x}_3 + \frac{1}{C_f \bar{L}_f} u_1 + \frac{a_1}{C_f} \widetilde{\Delta} u_1 + \frac{1}{C_f} \tilde{d}_1. \quad (67)$$

Similarly, for the second flat output we can write

$$\ddot{y}_2 = -\frac{1}{C_f \bar{L}_f} \tilde{x}_4 + \frac{1}{C_f \bar{L}_f} u_2 + \frac{a_2}{C_f} \widetilde{\Delta} u_2 + \frac{1}{C_f} \tilde{d}_2. \quad (68)$$

Considering the auxiliary flat output, we obtain the following:

$$\begin{aligned} \dot{z}_1 = & 2\omega \bar{L}_f (1 + \rho_{Lf} \delta_{Lf}) (x_1 \dot{x}_1 + x_2 \dot{x}_2) \\ & - 2\omega \bar{C}_f (1 + \rho_{Cf} \delta_{Cf}) (x_3 \dot{x}_3 + x_4 \dot{x}_4). \end{aligned} \quad (69)$$

Using (16)–(19) one obtains the following:

$$\begin{aligned} \dot{z}_1 = & 2\omega \bar{L}_f (1 + \rho_{Lf} \delta_{Lf}) \left[ x_1 \left( \frac{1}{\bar{L}_f} u_1 - \frac{1}{\bar{L}_f} x_3 + a_1 \Delta u_1 + d_1 \right) \right. \\ & \left. + x_2 \left( \frac{1}{\bar{L}_f} u_2 - \frac{1}{\bar{L}_f} x_4 + a_2 \Delta u_2 + d_2 \right) \right] \\ & - 2\omega \bar{C}_f (1 + \rho_{Cf} \delta_{Cf}) \left[ x_3 \left( \frac{1}{\bar{C}_f} x_1 + d_3 \right) \right. \\ & \left. + x_4 \left( \frac{1}{\bar{C}_f} x_2 + d_4 \right) \right]. \end{aligned} \quad (70)$$

Rearranging (70) and using the approximated parameters, one may write the following:

$$\begin{aligned} \dot{z}_1 = & \left( -2\tilde{x}_1 \tilde{x}_3 \left( \frac{\omega \bar{L}_f (1 + \rho_{Lf} \delta_{Lf})}{\bar{L}_f} + \frac{\omega \bar{C}_f (1 + \rho_{Cf} \delta_{Cf})}{\bar{C}_f} \right) \right. \\ & - 2\tilde{x}_2 \tilde{x}_4 \left( \frac{\omega \bar{L}_f (1 + \rho_{Lf} \delta_{Lf})}{\bar{L}_f} + \frac{\omega \bar{C}_f (1 + \rho_{Cf} \delta_{Cf})}{\bar{C}_f} \right) \Big) \\ & + \left( \frac{2\omega \bar{L}_f (1 + \rho_{Lf} \delta_{Lf})}{\bar{L}_f} \tilde{x}_1 \right) u_1 \\ & + \left( \frac{2\omega \bar{C}_f (1 + \rho_{Cf} \delta_{Cf})}{\bar{L}_f} \tilde{x}_2 \right) u_2 \\ & + (2\omega \bar{L}_f (1 + \rho_{Lf} \delta_{Lf}) a_1 \tilde{x}_1) \widetilde{\Delta} u_1 \\ & + (2\omega \bar{L}_f (1 + \rho_{Lf} \delta_{Lf}) a_2 \tilde{x}_2) \widetilde{\Delta} u_2 \\ & + (2\omega \bar{L}_f (1 + \rho_{Lf} \delta_{Lf}) \tilde{x}_1) \tilde{d}_1 \\ & + (2\omega \bar{L}_f (1 + \rho_{Lf} \delta_{Lf}) \tilde{x}_2) \tilde{d}_2 \\ & - (2\omega \bar{C}_f (1 + \rho_{Cf} \delta_{Cf}) \tilde{x}_3) \tilde{d}_3 \\ & - (2\omega \bar{C}_f (1 + \rho_{Cf} \delta_{Cf}) \tilde{x}_4) \tilde{d}_4. \end{aligned} \quad (71)$$

Therefore, (67), (68), and (71) can be rewritten in the linearized compact form as follows:

$$\emptyset(\tilde{x}) = f(\tilde{x}) + g(\tilde{x})u + \underbrace{O(\tilde{x})\widetilde{\Delta}u + S(\tilde{x})\tilde{d}}_{\Delta(\tilde{x})} \quad (72)$$

where  $\emptyset = [\emptyset_1 \ \emptyset_2 \ \emptyset_3]^T = [\ddot{y}_1 \ \ddot{y}_2 \ \dot{z}_1]^T$  is the linearized dynamics and  $\Delta(\tilde{x}) = [\Delta_1 \ \Delta_2 \ \Delta_3]^T$  is an uncertain part so that we have

$$\begin{aligned} f(\tilde{x}) &= \begin{bmatrix} f_1 \\ f_2 \\ f_3 \end{bmatrix} \\ &= \begin{bmatrix} -\frac{1}{C_f \bar{L}_f} \tilde{x}_3 \\ -\frac{1}{C_f \bar{L}_f} \tilde{x}_4 \\ -2(\tilde{x}_1 \tilde{x}_3 + \tilde{x}_2 \tilde{x}_4) \left( \frac{\omega \bar{L}_f (1 + \rho_{Lf} \delta_{Lf})}{\bar{L}_f} + \frac{\omega \bar{C}_f (1 + \rho_{Cf} \delta_{Cf})}{\bar{C}_f} \right) \end{bmatrix} \end{aligned}$$



$$g(\tilde{x}) = \begin{bmatrix} g_1 \\ g_2 \\ g_3 \end{bmatrix} = \begin{bmatrix} \frac{1}{C_f L_f} & 0 \\ 0 & \frac{1}{C_f L_f} \\ \frac{2\omega \bar{L}_f (1 + \rho_{L_f} \delta_{L_f})}{L_f} \tilde{x}_1 & \frac{2\omega \bar{L}_f (1 + \rho_{L_f} \delta_{L_f})}{L_f} \tilde{x}_2 \end{bmatrix}. \quad (73)$$

### B. Decentralized SMC-Based Controllers Design

Based on the linearized model, the following virtual control parts can be defined:

$$\mathcal{V}_1 = f_1(\tilde{x}) + g_1(\tilde{x})u \quad (74)$$

$$\mathcal{V}_2 = f_2(\tilde{x}) + g_2(\tilde{x})u \quad (75)$$

$$\mathcal{V}_3 = f_3(\tilde{x}) + g_3(\tilde{x})u. \quad (76)$$

The following sliding surfaces are defined as follows:

$$\sigma_1 = (y_{p1} - y_1) + \underbrace{\mathcal{K}_1 \int_0^t (y_{p1} - y_1) dx}_{\mathcal{P}_1} \quad (77)$$

$$\sigma_2 = (y_{p2} - y_2) + \underbrace{\mathcal{K}_2 \int_0^t (y_{p2} - y_2) dx}_{\mathcal{P}_2} \quad (78)$$

$$\sigma_3 = (z_{p1} - z_1) + \underbrace{\mathcal{K}_3 \int_0^t (z_{p1} - z_1) dx}_{\mathcal{P}_3}. \quad (79)$$

Therefore, by constructing the following matrices:

$$\mathbb{Y} = [y_1 \ y_2 \ z_1 \ \mathcal{P}_1 \ \mathcal{P}_2 \ \mathcal{P}_3]^T \quad (80)$$

$$\mathbb{Y}_p = [y_{p1} \ y_{p2} \ z_{p1} \ 0 \ 0 \ 0]^T \quad (81)$$

we can write

$$\begin{bmatrix} \sigma_1 \\ \sigma_2 \\ \sigma_3 \end{bmatrix} = \begin{bmatrix} 1 & 0 & 0 & -\mathcal{K}_1 & 0 & 0 \\ 0 & 1 & 0 & 0 & -\mathcal{K}_2 & 0 \\ 0 & 0 & 1 & 0 & 0 & -\mathcal{K}_3 \end{bmatrix} \begin{bmatrix} y_1 \\ y_2 \\ z_1 \\ \mathcal{P}_1 \\ \mathcal{P}_2 \\ \mathcal{P}_3 \end{bmatrix} - \begin{bmatrix} y_{p1} \\ y_{p2} \\ z_{p1} \\ 0 & 0 & 0 \end{bmatrix}^T \quad (82)$$

or in the compact form

$$\sigma = \mathcal{K} [\mathbb{Y}_p - \mathbb{Y}]. \quad (83)$$

In order to determine the virtual control vector  $\mathcal{V} = [\mathcal{V}_1 \ \mathcal{V}_2 \ \mathcal{V}_3]^T$  based on SMC, we temporarily ignore the uncertain part  $\Delta(\tilde{x})$  in (72), to obtain the second-order derivatives of the flat outputs. Thus, we obtain the following:

$$\ddot{y}_1 = \mathcal{V}_1 \quad (84)$$

$$\ddot{y}_2 = \mathcal{V}_2$$

$$\ddot{y}_1 = \mathcal{V}_3$$

$$\mathcal{P}_1 = \int_0^t (y_{p1} - y_1) dx \Rightarrow \dot{\mathcal{P}}_1 = y_{p1} - y_1 \Rightarrow \ddot{\mathcal{P}}_1 = \dot{y}_{p1} - \dot{y}_1. \quad (86)$$

In the same way we have

$$\ddot{\mathcal{P}}_2 = \dot{y}_{p2} - \dot{y}_2 \quad (87)$$

$$\ddot{\mathcal{P}}_3 = \dot{y}_{p3} - \dot{y}_3. \quad (88)$$

Therefore

$$\ddot{\mathbb{Y}} = \begin{bmatrix} 0 & 0 & 0 & 0 & 0 & 0 \\ 0 & 0 & 0 & 0 & 0 & 0 \\ 0 & 0 & 0 & 0 & 0 & 0 \\ -1 & 0 & 0 & 0 & 0 & 0 \\ 0 & -1 & 0 & 0 & 0 & 0 \\ 0 & 0 & -1 & 0 & 0 & 0 \end{bmatrix} \begin{bmatrix} \dot{y}_1 \\ \dot{y}_2 \\ \dot{z}_1 \\ \dot{\mathcal{P}}_1 \\ \dot{\mathcal{P}}_2 \\ \dot{\mathcal{P}}_3 \end{bmatrix} + \begin{bmatrix} 1 & 0 & 0 \\ 0 & 1 & 0 \\ 0 & 0 & 1 \\ 0 & 0 & 0 \\ 0 & 0 & 0 \\ 0 & 0 & 0 \end{bmatrix} \begin{bmatrix} \mathcal{V}_1 \\ \mathcal{V}_2 \\ \mathcal{V}_3 \end{bmatrix} + \begin{bmatrix} 0 \\ 0 \\ 0 \\ y_{p1} \\ y_{p2} \\ y_{p3} \end{bmatrix} \quad (89)$$

or in the compact matrix form

$$\ddot{\mathbb{Y}} = \mathcal{M}\dot{\mathbb{Y}} + \mathcal{B}\mathcal{V} + \mathcal{C}. \quad (90)$$

By defining

$$\dot{\mathbb{Y}} = \mathbb{Z} \quad (91)$$

we get the following new dynamics:

$$\dot{\mathbb{Z}} = \mathcal{M}\mathbb{Z} + \mathcal{B}\mathcal{V} + \mathcal{C}. \quad (92)$$

For system of the form (92), we propose an SMC-based controller, making the control scheme robust against parameter variations and unknown inputs.

The derivative of the sliding surface (83), the reaching law, is

$$\begin{bmatrix} \dot{\sigma}_1 \\ \dot{\sigma}_2 \\ \dot{\sigma}_3 \end{bmatrix} = - \begin{bmatrix} q_{y1} & 0 & 0 \\ 0 & q_{y2} & 0 \\ 0 & 0 & q_{z1} \end{bmatrix} \begin{bmatrix} \text{sat}((y_{p1} - y_1)/\varepsilon) \\ \text{sat}((y_{p2} - y_2)/\varepsilon) \\ \text{sat}((z_{p1} - z_1)/\varepsilon) \end{bmatrix} - \begin{bmatrix} \mathfrak{S}_{y1}(\sigma_1) \\ \mathfrak{S}_{y2}(\sigma_2) \\ \mathfrak{S}_{z1}(\sigma_3) \end{bmatrix} \quad (93)$$

or in the matrix form

$$\dot{\sigma} = -\mathfrak{Q}\text{sat}\left(\frac{(\sigma_j - \mathcal{P}_j)}{\varepsilon}\right) - \mathfrak{S}(\sigma) \quad (94)$$

where  $\mathfrak{Q} = \text{diag}[q_{y1} \ q_{y2} \ q_{z1}]$ . Therefore, the control vector  $\mathcal{V}$  must satisfy the following equation:

$$\mathcal{V} = [\mathcal{K}\mathcal{B}]^{-1} \left[ -\mathcal{K}\mathcal{M}\mathbb{Z} - \mathcal{K}\mathcal{C} - \mathfrak{Q}\text{sat}\left(\frac{(\sigma_j - \mathcal{P}_j)}{\varepsilon}\right) + \mathfrak{Q}\mathcal{K}(\mathbb{Y}_p - \mathbb{Y}) \right]. \quad (95)$$

After some manipulation, and using (80), (81), (90)–(92), and using (74)–(76), the actual control signals are as follows:

$$\mathbf{u} = \mathbf{g}^{-1}(\tilde{x}) [\mathcal{V} - \mathbf{f}(\tilde{x})]. \quad (96)$$

The proof of the robustness of such controllers are described in [23] and [24].

Thus, based on Fig. 3, the actual reference control signal which is given to the SPWM block, is determined by implementing inverse Clarke Transformation

$$\begin{bmatrix} u_a^{\text{Ref}} \\ u_b^{\text{Ref}} \\ u_c^{\text{Ref}} \end{bmatrix} = \underbrace{\begin{bmatrix} 1 & 0 \\ -1/2 & \sqrt{3}/2 \\ -1/2 & -\sqrt{3}/2 \end{bmatrix}}_{\mathbb{C}^T} \begin{bmatrix} u_\alpha \\ u_\beta \end{bmatrix} = \begin{bmatrix} 1 & 0 \\ -1/2 & \sqrt{3}/2 \\ -1/2 & -\sqrt{3}/2 \end{bmatrix} \begin{bmatrix} u_1 \\ u_2 \end{bmatrix}. \quad (97)$$

In the matrix compact style, we have the following:

$$\mathbf{u}_{abc}^{\text{Ref}} = \mathbb{C}^T \mathbf{u}. \quad (98)$$

Note that one should distinguish between the two defined controlled variables;  $\mathbf{U}_{abc}$  in (4) is the controlled output voltage of the BILPC whereas  $\mathbf{u}_{abc}^{\text{Ref}}$  is the reference control signal which is applied to the SPWM unit to provide  $\mathbf{U}_{abc}$ . These two parameters

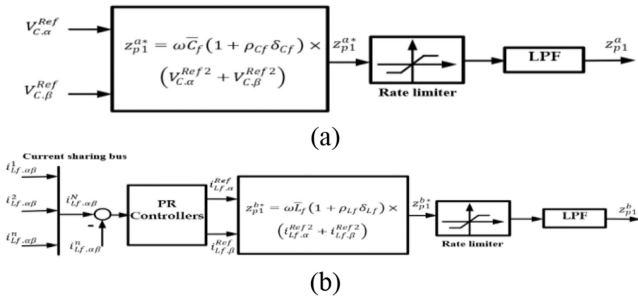


Fig. 6. Proposed desired trajectory planning for auxiliary flat output. (a) Planned electrostatic energy stored in filter capacitor. (b) Planned electromagnetic energy stored in filter inductor.

are related to each other through the duty cycle of the BILPC. Actually

$$U_{abc} = D^{-1} \mathbf{u}_{abc}^{Ref} \quad (99)$$

where  $D$  is a coefficient pertaining to the duty cycle.

### C. Desired Trajectories Determination

One of the main features of flatness-based control strategies is that the desirable outputs' trajectories can be predefined when designing the decentralized controllers. To this end, according to Fig. 3, we set the voltages  $y_{p1} = V_{\alpha}^{Ref}$  and  $y_{p2} = V_{\beta}^{Ref}$  as planned outputs for the first two flat outputs. For planning the desired trajectory for the auxiliary flat output  $z_{p1}$ , we propose the planning scheme indicated in Fig. 6. As shown, two PI controllers are implemented to generate the desired trajectory. As indicated in Fig. 6(a), the desired electrostatic energy stored in the filter capacitor is determined based on the planned first two flat outputs. On the other hand, as depicted in Fig. 6(b), the desired electromagnetic energy stored in the filter inductor is obtained based on a current sharing bus. The inductor current of each BILPC is given to the current sharing bus. The averaged residual current is  $i_{Lf,\alpha\beta}^N$ . The difference of  $i_{Lf,\alpha\beta}^N$  with the current of each BILPC, for example, BILPC number  $n$ , is given to the PR compensators to generate the reference current of each BILPC. In this way, each BILPC tries to reduce the residual current by regulating its output, resulting an appropriate current and power sharing among parallel-connected BILPCs. Therefore, using a low-pass filter with time constant  $\tau_0$ , according to Fig. 6, we have the following:

$$z_{p1} = -z_{p1}^a + z_{p1}^b. \quad (100)$$

## V. SIMULATION RESULTS AND DISCUSSION

The proficiency of the new flatness-based AHGPIO control strategy for BILPCs in an HMG is evaluated using simulation and competitive studies in MATLAB. An exemplary HMG with the topology indicated in Fig. 1 is considered. The HMG includes one dc subgrid and one ac subgrid. The dc subgrid contains a 250-kW PV unit accompanied with 50-kW battery, their specifications can be found in [20]. In the ac subgrid, there is a  $5 \times 50$  kW doubly fed induction generator (DFIG)-based wind unit, its specifications are given in [28]. The subgrids have their own regional loads. As illustrated, the subgrids are connected together using parallel-connected BILPCs. For comparison reasons, the

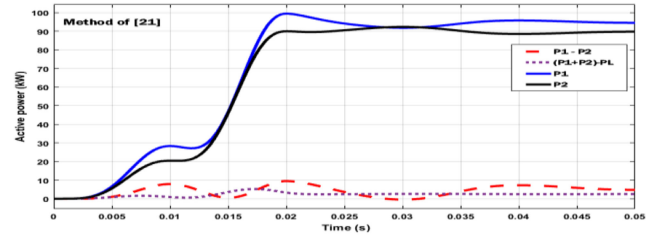


Fig. 7. Active powers of BILPCs using control method of [21].

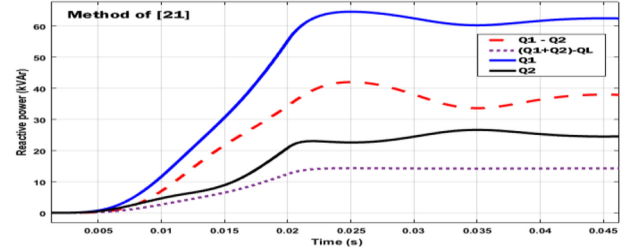


Fig. 8. Reactive powers of BILPCs using method of [21].

method of [21] is discussed in a similar system circumstance. The performance of the new control strategy and the control strategy of [21] are evaluated during a load change in the ac subgrid, while the resistance of line 1 is varied. The voltage of the dc bus is 470 V.

The dc subgrid is loaded with a 50-kW pure resistive load. All the arrays of the PV system are active, and therefore, the generated power in the dc subgrid is 250 kW and there is no load in the ac subgrid. Thus, no power is exchanged between the two microgrids. In the ac subgrid, one of the wind units is active, when a passive load  $S_{Load} = 250 \text{ kW} + 160 \text{ kVar} = 296.81 \angle 32.61^\circ \text{ kVA}$  is loaded at  $t = 2.5 \text{ ms}$ . Therefore, the main grid and the dc subgrid (since it provides a surplus power) are responsible for compensation of the needed power in the ac subgrid. Figs. 7 and 8 indicate the results when the BILPCs are equipped with the control strategy described in [21]. According to Fig. 7, the active powers of BILPC1 and BILPC2 are  $P_1 = 95 \text{ kW}$ , and  $P_2 = 90 \text{ kW}$ , respectively. Therefore, the active power difference is 5 kW. The lost active power in the transmission lines is  $(P_1 + P_2) - P_{L,BILPCs} = 4 \text{ kW}$ . Therefore, the transferred power from the dc subgrid to the ac subgrid is  $P_{L,BILPCs} = 181 \text{ kW}$ . The residual of the needed active power is provided by the power system and the wind turbine, i.e.,  $250 - 181 = 69 = P_{grid} + P_{1 \times 50 \text{ kW}}$ . Thus, 19 kW is injected by the power system. Fig. 8 illustrates the reactive powers. As shown,  $Q_1 = 63.7 \text{ kVar}$  and  $Q_2 = 24.9 \text{ kVar}$ ; thus, the difference is 38.2 kVar. The wasted reactive power is  $(Q_1 + Q_2) - Q_{L,BILPCs} = 14 \text{ kVar}$ . Thus, the BILPCs supply  $Q_{L,BILPCs} = 74.6 \text{ kVar}$  of the needed in the ac subgrid. The residual of the needed reactive power is injected by the power system and the DFIG. As demonstrated in Figs. 7 and 8, it is evident that the method of [21] is not capable of administrating proper power distribution for the power converters.

Figs. 9 and 10 show the simulation results in the same condition when the proposed control scheme is applied to BILPCs. The results validate the well-distribution of power among BILPCs. Fig. 9 indicates that the active power difference is less than 0.2 kW. For the power converts 1 and 2,  $P_1 = 95 \text{ kW}$ , and  $P_2 = 94.82 \text{ kW}$ ,

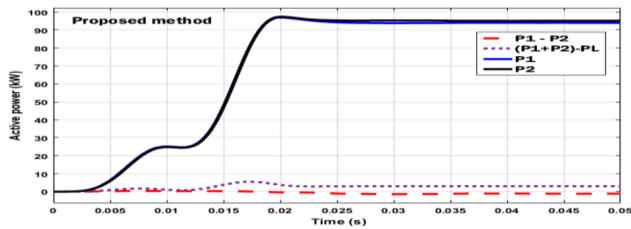


Fig. 9. Active powers of BILPCs using proposed control method.

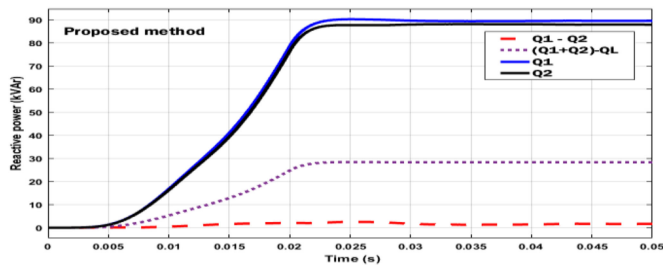


Fig. 10. Reactive powers of BILPCs using proposed control method.

respectively. Also,  $(P_1 + P_2) - P_{L,BILPCs} = 3.2$  kW, thus  $P_{L,BILPCs} = 186.62$  kW. Fig. 10 illustrates the reactive power distribution. As illustrated,  $Q_1 = 90$  kVar and  $Q_2 = 88.76$  kVar; thus, the difference is 1.24 kVar, which is noteworthy when comparing with Fig. 8. Furthermore,  $(Q_1 + Q_2) - Q_{L,BILPCs} = 29$  kVar and thus,  $Q_{L,BILPCs} = 149.76$  kVar.

Comparing the results, it is seen that the new control method has been able to reduce the active and reactive power discrepancies by 96%, and 96.75%, respectively. Furthermore, comparing  $P_{L,BILPCs}$  and  $Q_{L,BILPCs}$ , it is evident that the new method has resulted in enhanced the transferred power among the subgrids.

## VI. CONCLUSION

The control problem of BILPCs in an HMG has been investigated in this article. The unmodeled dynamics have been considered on the inductor and capacitor of the output  $LC$  filter, meanwhile the unknown input signals have been modeled in the main control signal of the BILPCs. Considering these unmodeled dynamics and unknown inputs, an AHGPIO has been designed to approximate these uncertain parts and unmeasured states. The approximated parameters have been used in I/O linearization of the BILPC model and based on this model, the SMC-based decentralized controllers have been designed. The desired trajectories have been planned based on the flatness feature of the BILPC model. The simulation results and case studies comparison have revealed the effectiveness of the proposed control scheme in controlling of BILPCs when the system condition changes.

## REFERENCES

- [1] A. Aderibole, H. H. Zeineldin, M. S. El-Moursi, J. C. Peng, and M. A. Hosani, "Domain of stability characterization for hybrid microgrids considering different power sharing conditions," *IEEE Trans. Energy Convers.*, vol. 33, no. 1, pp. 312–323, Mar. 2018.
- [2] A. A. Ejajal, A. H. Yazdavar, E. F. El-Saadany, and K. Ponnambalam, "On the loadability and voltage stability of islanded AC–DC hybrid microgrids during contingencies," *IEEE Syst. J.*, vol. 13, no. 4, pp. 4248–4259, Dec. 2019.
- [3] Nan Xia, H. B. Gooi, S. Chen, and W. Hu, "Decentralized state estimation for hybrid AC/DC microgrids," *IEEE Syst. J.*, vol. 12, no. 1, pp. 434–443, Mar. 2018.
- [4] M. Zolfaghari, M. Abedi, and G. B. Gharehpetian, "Power flow control of interconnected AC–DC microgrids in grid-connected hybrid microgrids using modified UIPC," *IEEE Trans. Smart Grid*, vol. 10, no. 6, pp. 6298–6307, Nov. 2019.
- [5] A. Firdaus and S. Mishra, "Mitigation of power and frequency instability to improve load sharing among distributed inverters in microgrid systems," *IEEE Syst. J.*, vol. 14, no. 1, pp. 1024–1033, Mar. 2020.
- [6] X. Lu, J. Guerrero, R. Teodorescu, T. Kerekes, K. Sun, and L. Huang, "Control of parallel-connected bidirectional AC–DC converters in stationary frame for microgrid application," in *Proc. IEEE Energy Convers. Congr. Expo.*, 2011, pp. 4153–4160.
- [7] X. Lu, J. M. Guerrero, K. Sun, J. C. Vasquez, R. Teodorescu, and L. Huang, "Hierarchical control of parallel AC–DC converter interfaces for hybrid microgrids," *IEEE Trans. Smart Grid*, vol. 5, no. 2, pp. 683–692, Mar. 2014.
- [8] R. Rajan and F. M. Fernandez, "Power control strategy of photovoltaic plants for frequency regulation in a hybrid power system," *Int. J. Elect. Power Energy Syst.*, vol. 110, pp. 171–183, 2019.
- [9] M. Zolfaghari, H. B. Habel, H. A. Abyaneh, and M. Abedi, "Load sharing improvement between parallel-connected inverter based DGs using a GA based optimization control strategy in microgrids," in *Proc. IEEE PES Asia-Pac. Power Energy Eng. Conf.*, 2016, pp. 320–323.
- [10] X. Liu, P. Wang, and P. C. Loh, "A hybrid AC/DC microgrid and its coordination control," *IEEE Trans. Smart Grid*, vol. 2, no. 2, pp. 278–286, Jun. 2011.
- [11] P. Yang, Y. Xia, M. Yu, W. Wei, and Y. Peng, "A decentralized coordination control method for parallel bidirectional power converters in a hybrid AC–DC microgrid," *IEEE Trans. Ind. Electron.*, vol. 65, no. 8, pp. 6217–6228, Aug. 2018.
- [12] F. Nejbatkhal, Y. W. Li, and K. Sun, "Parallel three-phase interfacing converters operation under unbalanced voltage in hybrid AC/DC microgrid," *IEEE Trans. Smart Grid*, vol. 9, no. 2, pp. 1310–1322, Mar. 2018.
- [13] M. Baharizadeh, H. R. Karshenas, and J. M. Guerrero, "Control strategy of interlinking converters as the key segment of hybrid AC–DC microgrids," *IET Gener., Transmiss. Distrib.*, vol. 10, no. 7, pp. 1671–1681, 2016.
- [14] P. C. Loh, D. Li, Y. K. Chai, and F. Blaabjerg, "Autonomous control of interlinking converter with energy storage in hybrid AC–DC microgrid," *IEEE Trans. Ind. Appl.*, vol. 49, no. 3, pp. 1374–1382, May/Jun. 2013.
- [15] N. M. Dehkordi, N. Sadati, and M. Hamzeh, "Robust backstepping control of an interlink converter in a hybrid AC/DC microgrid based on feedback linearisation method," *Int. J. Control*, vol. 90, no. 9, pp. 1990–2004, 2017.
- [16] H. Zhang, J. Zhou, Q. Sun, J. M. Guerrero, and D. Ma, "Data-driven control for interlinked AC/DC microgrids via model-free adaptive control and dual-droop control," *IEEE Trans. Smart Grid*, vol. 8, no. 2, pp. 557–571, Mar. 2017.
- [17] M. S. Rahman, M. J. Hossain, F. H. M. Rafi, and J. Lu, "A multi-purpose interlinking converter control for multiple hybrid AC/DC microgrid operations," in *Proc. IEEE Innovative Smart Grid Technologies Asia*, 2016, pp. 221–226.
- [18] S. Manju, P. N. Seema, and A. Rajendran, "A novel algorithm for power flow management in Combined AC/DC microgrid," in *Proc. IEEE 1st Int. Conf. Power Electron., Intell. Control Energy Syst.*, 2016, pp. 1–6.
- [19] S. A. Taher and M. Zolfaghari, "Designing robust controller to improve current-sharing for parallel-connected inverter-based DGs considering line impedance impact in microgrid networks," *Int. J. Elect. Power Energy Syst.*, vol. 63, pp. 625–644, 2014.
- [20] M. Fliess, J. Levine, P. Martin, and P. Rouchon, "A Lie-Backlund approach to equivalence and flatness of nonlinear systems," *IEEE Trans. Autom. Control*, vol. 44, no. 5, pp. 922–937, May 1999.
- [21] M. Fliess, J. LÉVine, P. Martin, and P. Rouchon, "Flatness and defect of non-linear systems: introductory theory and examples," *Int. J. Control*, vol. 61, no. 6, pp. 1327–1361, 1995.
- [22] F. Bakhshande and D. Söffker, "Proportional-integral-observer: A brief survey with special attention to the actual methods using ACC Benchmark," *IFAC-PapersOnLine*, vol. 48, no. 1, pp. 532–537, 2015.
- [23] M. Zolfaghari, S. H. Hosseini, S. H. Fathi, M. Abedi, and G. B. Gharehpetian, "A new power management scheme for parallel-connected PV systems in microgrids," *IEEE Trans. Sustain. Energy*, vol. 9, no. 4, pp. 1605–1617, Oct. 2018.
- [24] S. A. Taher, M. Zolfaghari, C. Cho, M. Abedi, and M. Shahidehpour, "A new approach for soft synchronization of microgrid using robust control theory," *IEEE Trans. Power Del.*, vol. 32, no. 3, pp. 1370–1381, Jun. 2017.